ANALYSIS OF FIBROUS FELTS FOR FLEXIBLE ABLATORS USING SYNCHROTRON HARD X-RAY MICRO-TOMOGRAPHY

Francesco Panerai [(1)], Joseph Ferguson[(1)], Jean Lachaud [(3)], Alexandre Martin [(1)], Matthew J. Gasch [(2)], Nagi N. Mansour [(2)]

[(1)] University of Kentucky, Lexington, KY 40506, USA, Email: francesco.panerai@uky.edu
[(2)] NASA Ames Research Center, Moffett Field, CA 94035, USA
[(3)] University of California Santa Cruz, Santa Cruz, CA 95064, USA

ABSTRACT

We analyzed the material properties of low-density felts that are used as substrates for new-generation flexible and conformal carbon/phenolic ablators, and compared them with those of a rigid carbon fiber preform that is used to manufacture rigid carbon/phenolic ablators. Micro-tomography measurements were obtained using synchrotron X-rays, allowing the characterization of the materials' microstructure at the scale of the fibers. Using the tomography voxels as computational grids, we computed tortuosity and room temperature conductivity. In addition we performed micro-scale simulations of the oxidation of carbon fibers using a random walk model for oxygen diffusion and a probability law to model surface reactions.

1. INTRODUCTION

The successful atmospheric entries of Stardust, Mars Science Laboratory (MSL) and the recent flights of the SpaceX Dragon capsule have demonstrated a substantial maturity and performance of lightweight carbon/phenolic thermal protection systems (TPS) with densities much lower than fully dense carbon/phenolic (1.45 g/cm^3). This class of lightweight ablators has proven capable of handling the aerothermal heating of different atmospheric environments and wide ranges of entry speeds.

In order to prepare for future exploration missions and to meet the more demanding thermal protection requirements of re-entries from beyond Low Earth Orbit (LEO), NASA is investing in both improving material response models for low-density carbon/phenolic ablators and developing new material technologies that enable better performance and more effective design. Examples are conformal and flexible carbon/phenolic composites. These materials are manufactured by infusion of a phenolic resin in a fibrous substrate. Such a process is based on the heritage of Phenolic Impregnated Carbon Ablator (PICA), which is the current state-of-the-art in low-density TPS materials. However, unlike PICA, which is based on a rigid preform (FiberForm), the new materials adopt flexible felts as the material substrate. Felt substrates suitable for flexible and conformal ablators are based on ceramic, polymers or carbon fibers. Conformal PICA, made according to this process, using a carbon felt impregnated with phenolic, was tested with success in an arcjet environment at heat fluxes ranging from 50 to 385 W/cm^2 [1].

Felt-based ablators have several advantages over classical rigid TPS. Most importantly, they mitigate the limited strain capability of large rigid substrates. For example, Shuttle tiles and heritage PICA, due to their brittleness, need to be manufactured as tiles of limited dimensions. That was the case for the large PICA heat shield of MSL. Felts have significantly larger strain-to-failure than rigid preforms, therefore they enable manufacturing of carbon/phenolic TPS materials in larger pieces. They also reduce the number of independent parts, mitigating the need of gap fillers, and they offer improved robustness in absorbing loads and deflections. Furthermore, the flexibility of felts allows for an easier shaping of the substrate around more complex geometrical shapes, with the possibility of maintaining a uniform, low, through-the-thickness thermal conductivity, in presence of curved surfaces [1].

In this paper, we analyze the differences in material properties of rigid and flexible substrates utilized in lightweight carbon/phenolic ablators. Understanding the microscale properties of the substrate or preform material is very informative for multiple reasons. An accurate characterization of the microstructure can inform detailed models of the decomposition of the fibers, at the stage of ablation where the polymer matrix is fully pyrolized and has left the substrate exposed to the reactive flow. This understanding may enable detailed modeling of the heat and mass transport through the porous medium. It could also provide useful information to improve infiltration of the substrate sand about the distribution of the different resin within the substrate, which has a strong impact on the properties of the material.

We used synchrotron X-ray micro-tomography (micro-CT) to characterize the microstructural properties of both felts and rigid preform. Micro-CT measurements provide highly resolved information on the material structure. Compared to a standard scanning electron microscope characterization, micro-CT adds the possibility of visualizing the material in three

dimensions and provides a digital representation of the material as a set of voxels that can be used for numerical simulations. Here the micro-CT data were imported into the GeoDict frame, a commercial toolbox to perform computations of materials properties, and into PuMA (Porous Materials Analysis), a NASA's software for microscale oxidation simulations.

2. MICRO-TOMOGRAPHY OF RIGID CARBON PREFORM AND FLEXIBLE FELT.

Micro-CT measurements were performed at the Advanced Light Source (ALS) at Lawrence Berkeley National Laboratory. Synchrotron X-rays produced by the ALS provide high quality images, with low noise and sub-micron resolution. This is ideal for resolving the fibrous architecture of highly porous substrates.

The tomography setup and its capabilities are described in [2]. In this study, to collect tomography images, we used a 2560×2160 pixels pco.edge 5.5 sCMOS camera (PCO, Kelheim, Germany) and a 10× Mitutoyo Plan Apo long working distance objective (Mitutoyo, Kawasaki, Japan) providing a pixel size of 0.645 µm. The scans were performed at an X-ray energy of 18 keV. Micro-CT projections were reconstructed into 3D images using the Octopus software (inCT, Aalst, Belgium) [3], using an ALS in-house interface implemented in the Fiji software [4]. Fiji was also used to filter tomography artifacts and segment the images for visualization.

We imaged samples of FiberForm™ (Fiber Materials Inc., Biddeford, ME, USA), carbon felt and rayon felt. FiberForm is the carbon substrate used in PICA. It is made from a slurry composed of chopped rayon-based carbon fibers mixed with phenol-formaldehyde resin and water. The slurry is vacuum casted, compressed and cured at high temperature into desired shapes. Of the conformal and flexible materials being developed at NASA Ames Research Center (ARC), two different felts were considered. The materials analyzed were a low-density rayon-based carbon fiber felt from Morgan Advanced Material (Windsor, Cornwall, UK) and a needled (densified) rayon fiber felt from the American Felt & Filter Company (AFFCO, New Windsor, NY, USA). The rayon was made of semisynthetic fibers derived from cellulose. Felts fabrics were made by a combination of mechanical, chemical and thermal treatments that are proprietary to each manufacturer.

Photorealistic renderings of FiberForm and the carbon felt are shown in Figure 1. The visualizations were produced from triangulated micro-CT data, at the NASA Ames Advanced Supercomputing facilities, using ray-tracing [5]. The figure highlights appreciable differences between FiberForm and the Morgan felt.

Fiber diameters (≈10-12 µm) and aspect ratio of the two materials are similar, as both the carbon felt and FiberForm's fibers are rayon based. However, while FiberForm presents numerous clumps, cluster and bundles of fibers due to the FMI manufacturing process, these are not present in the felt. The carbon felt fibers appear to be organized in a more regular architecture that follows a defined pseudo-weaving pattern. This can be observed in Fig. 1(b), showing a clear needling pattern.

The felts investigated in this study are more porous than FiberForm, as can be noticed from the visualization in Figure 1. An analysis of the gray-scale distribution of the tomography voxels revealed porosities of ≈85 to 89% for FiberForm, while higher than ≈94% for fibrous felts.

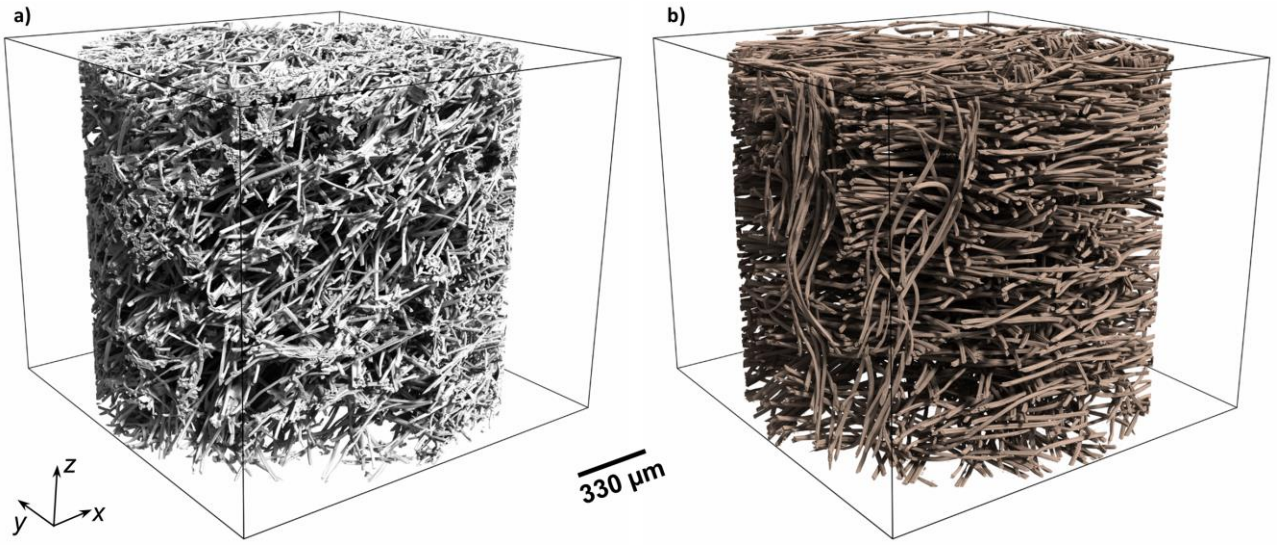


Figure 1. Micro-CT ray-tracing rendering of a) FiberForm and b) Morgan carbon-fiber felt. Here and in following sections x- y define the "in-plane" direction and z the "through-the-thickness" direction.

3. MATERIAL PROPERTIES ANALYSIS

The GeoDict software was used to perform analyses of material properties. Filtered micro-CT data were imported into the software, segmented and visualized using the OpenGL ray-casting feature of GeoDict. The computational domains are presented in Figure 2: a) FiberForm, b) carbon felt, c) needled rayon felt. As an ensemble of voxels, the micro-CT data can be used directly as a computational Cartesian grid. After segmentation, the colored voxels correspond to the fibrous material, while the white volume represents the voids between them. Prior to importing into GeoDict, we scaled the micro-CT datasets by half (resulting in a voxel size of 1.29 µm), and extracted sub-volumes of ≈1 mm^3 (800^3 voxels). Scaling the data has the advantage of allowing computations on large, representative volumes while keeping computational costs down. As an example, effective conductivity tensor calculations, performed on the half billion voxel datasets, required a computational time on the order of 1 h using 4 threads of a workstation. Comparisons of visualizations, porosities and surface areas values of down-sampled models with the original datasets confirmed negligible loss of information and computational errors.

3.1. Tortuosity

Tortuosity is a geometrical parameter that describes the random trajectory of fluid particles within a porous medium. In modelling porous ablators, this parameter is important as it is used to compute the effective diffusion coefficient for the mass conservation of diffusing species [6]. The effective diffusion coefficient for a porous medium reads:

$$D_{\text{eff}} = \frac{\varepsilon}{\eta} D_{\text{ref}} \tag{1}$$

where ε is the porosity, D_{ref} is the reference diffusivity (that of the straight capillary) and η tortuosity factor [7]. The ε/η ratio is also called dimensionless diffusivity D^*. The reference diffusion coefficient reads differently depending on what the flow regime is. For a porous material, the Knudsen number Kn can be defined as the ratio of the fluid particles mean free path $\bar{\lambda}$ to the mean pore diameter d_p. For small Knudsen numbers (Kn $\ll 1$, Laplace regime), the voids are large compared to the mean free path; hence diffusion in the pores is controlled by collisions between the molecules. Within a PICA-like ablator this flow regime may be experienced in the later portion of the trajectory, where temperatures are lower and pressures higher (note that, for instance, the mean free path of oxygen-in-air scales proportionally to the T/P ratio [6]). Conversely, for large Knudsen numbers (Kn $\gg 1$, Knudsen regime), typical of an early portion of the entry phase, the pore diameters are small compared to the mean free path. In this case diffusion is ruled by collisions of the fluid particles with the solid boundaries. In the case of a

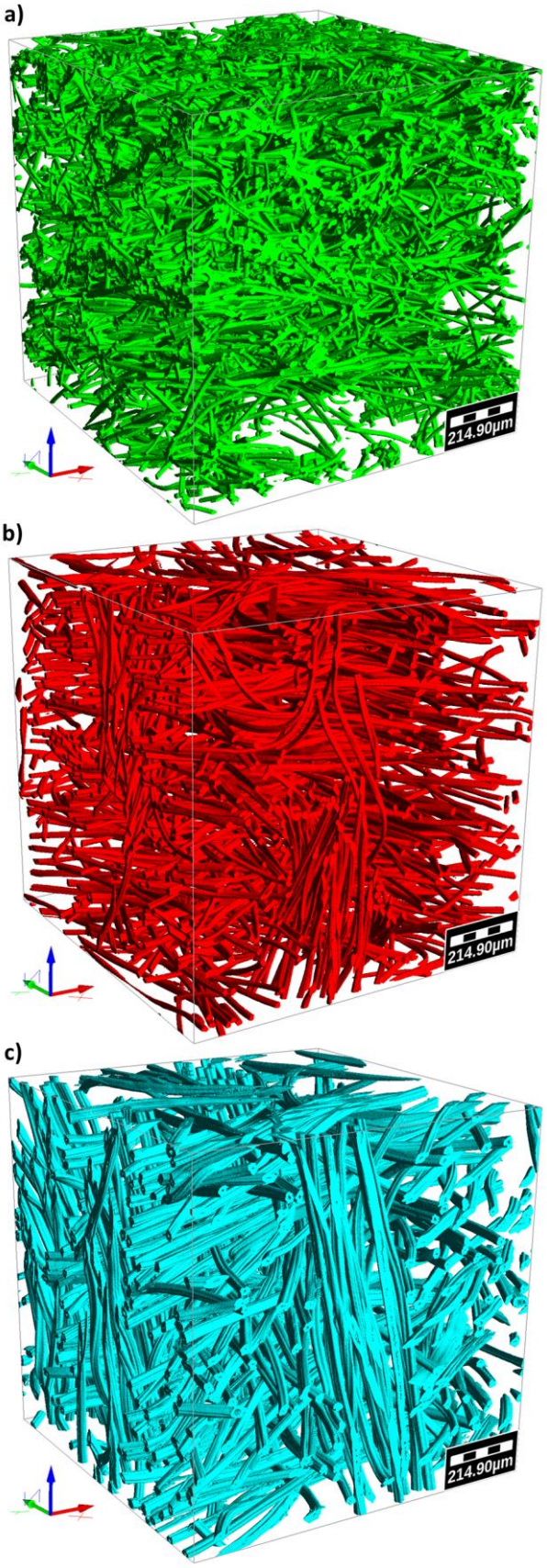


Figure 2. GeoDict computational domains from micro-CT voxels: a) FiberForm, b) carbon felt and c) rayon felt.

single gas, e.g. a pure O_2 flow, the bulk and Knudsen reference self-diffusion coefficients read respectively as $D_{bulk} = \frac{1}{3}\lambda\bar{v}$ and $D_{Kn} = \frac{1}{3}d_p\bar{v}$ [6]. Here $\bar{v}$ is the mean thermal velocity of the gas. For transition regimes, the Bosanquet approximation applies [6]:

$$D_{\text{ref}}^{-1} = D_{bulk}^{-1} + D_{Kn}^{-1} \quad (2)$$

The DiffuDict module of GeoDict was used to perform diffusion coefficients calculations for Fiberform, carbon felt and rayon felt. For the calculation of the diffusion coefficient in the continuum case, DiffuDict solves the Laplace equation, while a random walk procedure is used in the rarefied regime [8]. Here, we limit calculations of the diffusivity and tortuosity to the continuum regime, leaving computations in the rarefied case for a future study.

Bulk tortuosities are plotted in Figure 3. They clearly show the orthotropic structure of the substrates with a more tortuous path in the z direction limiting the diffusion of species. The larger porosity of the felt materials compared to the rigid FiberForm gives a lower tortuosity with respect to the felts.

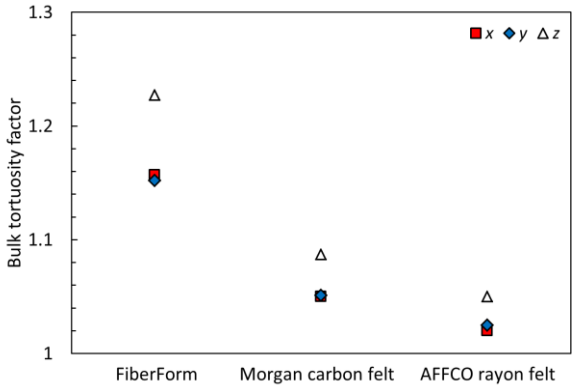


Figure 3. Bulk tortuosities for rigid and flexible substrate.

3.2. Room-temperature conductivity

Room-temperature conductivity computations were performed using the ConductoDict module of GeoDict. The module solves Fourier's law at steady-state for composite material with complex architecture and with high contrast in the thermal conductivity of the composing phases [9]. Periodic boundary conditions were used and a scalar conductivity value for the different phases (carbon fibers and pores) of the material was imposed. The phases are assumed to be isotropic. Radiative transfer within the porous medium was not modeled. This is an acceptable approximation for the computations presented here, as only values at room temperature were considered. The code returns the effective conductivity tensor of the composite:

$$\underline{\underline{\mathbf{k}}} = \begin{pmatrix} k_{11} & k_{12} & k_{13} \\ k_{21} & k_{22} & k_{23} \\ k_{31} & k_{32} & k_{33} \end{pmatrix} \quad (3)$$

The diagonal values correspond to the conductivity values for the x, y and z direction respectively. The off-diagonal terms depend on the orientation of the material with respect to the main directions of conduction.

For the present simulations, we adopted conductivity values published in the literature for the single phases. For the gas phase, conductivities are well documented or easy to compute. For the fibers, assumptions are more involved, as the actual conductivity depends on the nanoscale architecture of the materials and might be anisotropic. However reasonable choices can be made based on the type of material. As FiberForm and Morgan carbon are both made of rayon-based fibers, we assumed a conductivity of $k_f = 12$ W/(mK) for their fibers. This is consistent with room-temperature values for rayon-based carbon fibers, which are found in the literature to be between 5 and 15 W/(mK) [10-12]. For the conductivity of the rayon felt fibers, we used a conductivity of $k_f = 1.89$ W/(mK) as given in [11].

For the three materials, we performed computations with void pores (null conductivity), air- and CO_2-filled pores, assuming conductivity at 293 K and 1 atm. For the CO_2 case (for FiberForm and carbon felt) we also computed conductivity at low pressure conditions typical of the early phase of a Martian entry maneuver.

As an example of ConductoDict output, the conductivity of FiberForm in air at standard conditions reads:

$$\underline{\underline{\mathbf{k}}}_{FiberForm} = \begin{pmatrix} 0.329 & -0.061 & -0.011 \\ -0.061 & 0.353 & -0.074 \\ -0.011 & -0.074 & 0.203 \end{pmatrix} \quad (4)$$

The value in the z direction is close to the nominal (maximum) room-temperature value of FiberForm conductivity, quoted by the manufacturer (0.21 W/(mK)). This gives confidence in our assumption of the fibers' conductivity. The tensor clearly highlights the orthotropic properties of FiberForm, where in-plane (x, y) conductivities are similar and higher than the through-the-thickness value (z). This is a result of the manufacturing process, where, as an effect of the compression of a FiberForm tile during molding, fibers tend to align with the plane of compression. The tensor in Eq. 4 can be assumed to be practically a diagonal matrix with an uncertainty of ±0.06 W/(mK).

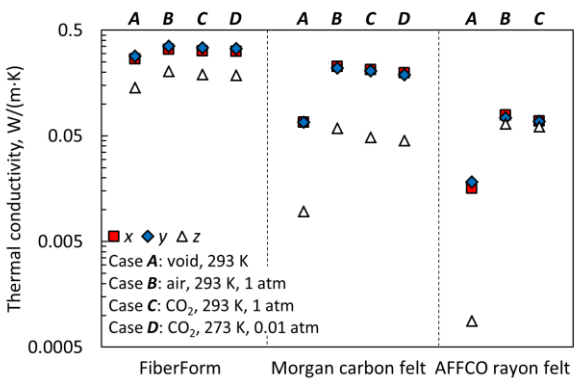


Figure 5. Comparison of room-temperature thermal conductivities of rigid and flexible substrates with different pore-filling gas.

Conductivity calculations are summarized in Figure 5. The three materials have orthotropic thermal properties with the lowest thermal conductivity in the through-the-thickness direction. The results highlight the importance of the gas state within the pores. Due to the effect of the gas conductivity, void pores yield the lowest conductivity. The percent difference in conductivity between void pores and gas-filled pores is higher for the higher porosity materials (felts) than FiberForm. For FiberForm, the through-the-thickness conductivity in CO_2 at standard conditions and CO_2 at low pressure is respectively ≈7 and ≈10% lower than that in air at standard conditions. In the case of the felts, the difference between air and CO_2 conductivities can be up ≈20%.

The z direction conductivity of FiberForm is one order of magnitude higher than the carbon felt and two orders of magnitude higher that the rayon felt. For the conductivities in the in-plane direction this difference is lower. Indeed, analyzing the data, if one considers the thermal-electrical analogy, due to the preferential orientation of the fibers with the x-y plane, for the in-plane direction the conductivities of the different phases would nearly behave as resistances in parallel. Hence the effective conductivity would scale as the sum of the conductivities of the different phases. Conversely in the though-the-thickness direction they would behave as resistance in series, where the reciprocal effective conductivity is nearly the sum of the reciprocal conductivities of the single phases.

Observing the behavior of the conductivity for the rayon felt, one can also notice that the difference between the in-plane and through-the-thickness values is very small. This is due to the low conductivity of rayon. Since k_f is only slightly higher than that of the pore-filling gas, the introduction of the gas phase nearly eliminates the effect of the orthotropic structure.

In Figure 4 we artificially built two carbon/phenolic composites, using Fiberform and Morgan carbon felt as preforms. For the material based on FiberForm we randomly placed phenolic around the fibers and phenolic clusters within the pore for a total phenolic volume fraction of about 5.3% resulting in a bulk porosity of ≈82%. For the composite built upon the carbon felt we used a higher phenolic content, distributed around the fibers and in the voids, to have approximately the same density as the one based on FiberForm. We performed room-temperature conductivity calculations, using a conductivity of phenol formaldehyde resin of $k_p = 0.35$ W/(mK) from [13]. The voids are considered as air at standard conditions. The results are shown in Figure 6 together with FiberForm and carbon felt conductivities.

We notice that the addition of a phenolic phase causes a very small increase in conductivity compared to the substrate. For the felt-based material, with a high

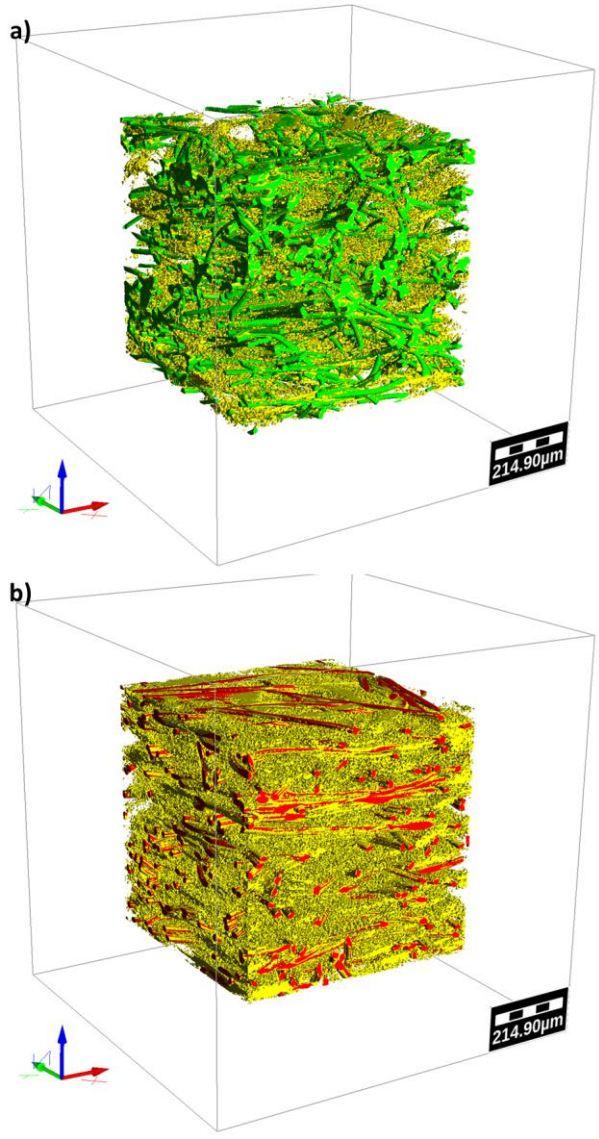


Figure 4. GeoDict computational domains of artificial composites: a) FiberForm + ≈5.3% phenolic , b) Morgan carbon felt + ≈12.5% phenolic.

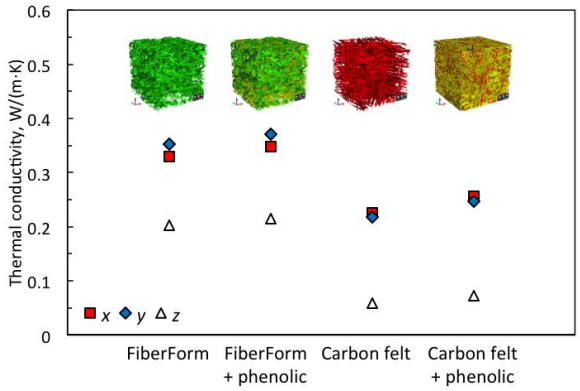


Figure 6. Comparison of room-temperature conductivity of substrates, and of substrates with phenolic loading.

phenolic loading, an increase in conductivity of only 22% with respect to the pure substrate is computed. The addition of the phenolic phase does not affect the orthotropy of the thermal properties. Such observation highlights that, as expected, the conductivity is primarily driven by the properties of the substrate. It is acknowledged here that the distribution of the phenolic is not representative of the real, nanodispersed phenolic phase of actual PICA-like composites, therefore these cases have to be purely considered as numerical examples. Even though the two digitally created materials are not meant to reproduce actual composites, these numerical tests show how, knowing the properties of the preform material and those of the phenolic phase, the bulk conductivity could be easily computed. One could also think of reversing the problem and using this numerical approach to engineer actual materials. For instance, one could numerically achieve a desired conductivity by tailoring distribution and/or the loading of the phenolic phase and then use such optimization to inform the actual material manufacturing.

4. MICROSCALE OXIDATION SIMULATIONS

In this section we analyze and compare the microscale oxidation of FiberForm and carbon felt. Simulations were performed to investigate the decomposition of carbon fibers due to their interaction with oxygen reactants. The simulations were executed using PuMA, a software under development at ARC for simulations based on tomography data. A description of the current PuMA capabilities will be presented in a forthcoming publication. Gasification of carbon fibers is modeled using a technique analogous to that presented in [14-16]. Mass transfer is simulated with random walks of

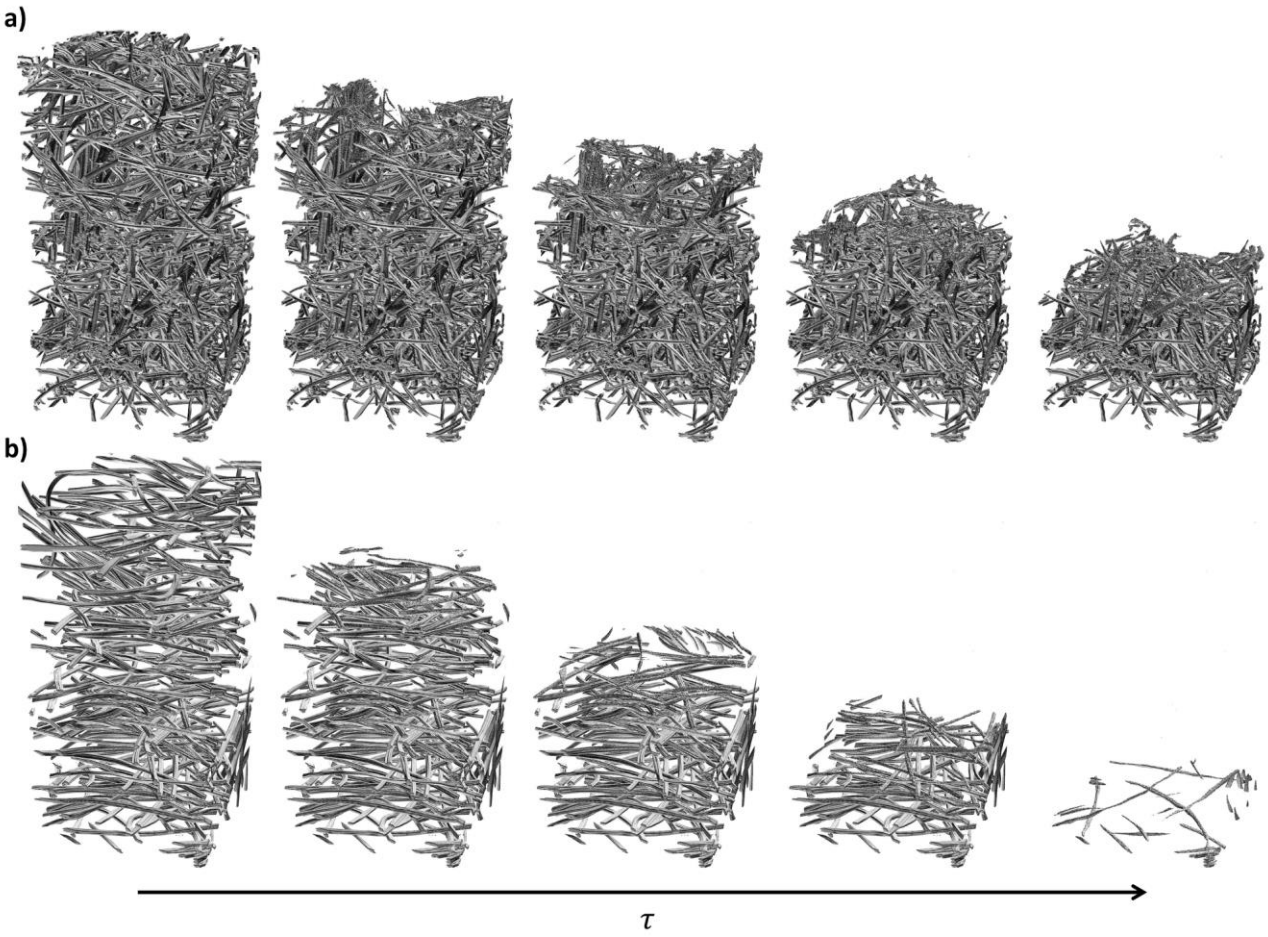


Figure 7. Time progression of a) FiberForm and b) Morgan carbon felt recession simulated with PuMA.

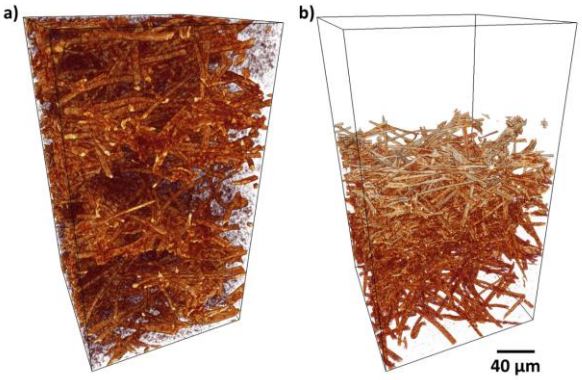


Figure 8 Micro-CT of a) virgin and b) ablated PICA. The ablated image has been acquired from the top surface of a sample tested in the NASA Langley HYMETS arcjet at 200 W/cm^2 heat flux, 0.05 atm stagnation pressure, for 30 s.

oxygen particles. The carbon/oxygen reactions and the consequent recession of the surface are modeled using a probability law with rates published in the literature. Each user-defined number of time steps the oxidized morphology of the material is segmented using a marching cubes algorithm and rendered with an OpenGL plugin implemented in PuMA.

The computations were performed on subsamples of the datasets displayed in Figure 1. We used 400×400×800 voxels volumes, with a voxel size of 1.29 µm microns. We tailored the simulation parameters to reproduce a surface ablation regime, where the timescale of the oxidation reactions is much smaller than that of the diffusion within the porous medium. In such conditions, the reactants are mostly consumed near the top surface, and the amount of oxygen penetrating in depth is very small, due to the high reactivity of the fibers and the low diffusivity.

The same simulation parameters (carbon fiber reactivity and diffusion coefficient) were used for both FiberForm and carbon felt. This allows a one-to-one comparison of the two under the same conditions. It is reasonable to assume the same reactivity for the fibers, as both materials are made of rayon-based carbon fibers. Using the same diffusion coefficient ensures the same oxygen transport.

Figure 7 shows the time progression of the decomposition of the two materials. Still images were extracted at exactly the same time interval for the two materials. It is clearly observed that, due to its lower density, the carbon felt ablates much faster than FiberForm. We estimated a volumetric recession rate of $\approx 1.4\times10^{-3}$ mm^3/s for FiberForm compared to $\approx 2.3\times10^{-3}$ mm^3/s for the carbon felt.

The surface ablation conditions reproduced by the present simulations typically occur during high heat flux testing at conditions >300 W/cm^2. At the surface of the specimen the phenolic phase, which is more reactive than the carbon fibers, decomposes faster and leaves the carbon fibers of the substrate exposed to the freestream reactants. Oxygen atoms react at the surface and lead to the recession of the materials. In Figure 8 we present the micro-CT scan of virgin PICA, compared to that of the top surface of a PICA sample, tested in arcjet environment. The visualizations were produced using the Avizo 8.0 software (FEI Visualization Sciences Group, Burlington MA, USA). While the "fluffy" phenolic phase is seen in the image of the virgin material, only carbon fibers are resolved in the scan of the ablated sample. The fibers have a typical needle shape observed during high temperature ablation in diffusion-limited regimes. Indeed, the image of the ablated sample qualitatively resembles the oxidized FiberForm shown in the last frame of Figure 7a. A quantitative comparison of images could be used to infer material properties of the ablated PICA surface. Assuming that the diffusion coefficient of an arcjet test could be accurately known, one could adjust the effective reactivity of the carbon fibers in PuMA to match density and specific surface area of the actual ablated sample. The results could then be used to estimate the effective fiber reactivity at the actual test temperature of the arcjet model.

5. OUTLOOK

We presented a comparison of flexible fibrous felts to a rigid substrate used in the fabrication of carbon/phenolic composites. Microscale oxidation simulations provided evidence of the faster recession of a carbon felt compared to rigid FiberForm, consistent with a higher recession of C-PICA, observed experimentally during arcjet testing, compared to PICA. We showed the capability of using micro-CT imaging for computing material properties as tortuosity and conductivity and showed that felts have significantly lower room-temperature conductivity than FiberForm as observed experimentally. The availability of 3D digital description of the microstructure leads to the possibility of computing high temperature thermal properties by simulating radiative heat transfer within the porous medium. The use of Direct Simulation Monte Carlo methods will enable computation in rarefied regime using advanced chemistry models for the gas/surface interactions at the fibers surface.

We showed that microscale imaging can be used in predictive simulations that could also help in the manufacturing ablative materials with tailored and/or optimized properties.

ACKNOWLEDGEMENTS

This work was performed under the Fundamental Aeronautics Hypersonics EDL program (Drs. M.J. Wright and A.M. Calomino). Support to Francesco Panerai was provided by NASA and Kentucky EPSCoR Award NNX13AN04A and NASA Award

NNX14AI97G. The authors would like to acknowledge the contribution of T.A. Sandstrom for the ray-tracing rendering of the micro-CT data. The commitment of the Advanced Light Source beamline scientists Drs. A.A. McDowell and D.Y. Parkinson in the collaborative effort with NASA Ames is gratefully acknowledged. The Advanced Light Source is supported by the Director, Office of Science, Office of Basic Energy Sciences, of the U.S. Department of Energy under Contract No. DE-AC02-05CH11231.

REFERENCES

1. Milos, F.S. & Gasch, M.J. (2015). Conformal Phenolic Impregnated Carbon Ablator (C-PICA) Arcjet Testing, Ablation and Thermal Response. In Proc. *53rd AIAA Aerospace Sciences Meeting*, American Institute of Aeronautics and Astronautics.
2. MacDowell, A.A., Parkinson, D.Y., Haboub, A., Schaible, E., Nasiatka, J.R., Yee, C.A., Jameson, J.R., Ajo-Franklin, J.B., Brodersen, C.R. & McElrone, A.J. (2012). In Proc.
3. Dierick, M., Masschaele, B. & Hoorebeke, L.V. (2004). Octopus, a fast and user-friendly tomographic reconstruction package developed in LabView®. *Meas. Sci. Technol.* **15**(7), 1366.
4. Schindelin, J., Arganda-Carreras, I., Frise, E., Kaynig, V., Longair, M., Pietzsch, T., Preibisch, S., Rueden, C., Saalfeld, S., Schmid, B., Tinevez, J.Y., White, D.J., Hartenstein, V., Eliceiri, K., Tomancak, P. & Cardona, A. (2012). Fiji: an open-source platform for biological-image analysis. *Nat. Methods.* **9**(7), 676-682.
5. Kajiya, J.T. (1986). The rendering equation. *SIGGRAPH Comput. Graph.* **20**(4), 143-150.
6. Lachaud, J., Cozmuta, I. & Mansour, N.N. (2010). Multiscale Approach to Ablation Modeling of Phenolic Impregnated Carbon Ablators. *J. Spacecraft Rockets* **47**(6), 910-921.
7. Epstein, N. (1989). On tortuosity and the tortuosity factor in flow and diffusion through porous media. *Chem. Eng. Sci.* **44**(3), 777-779.
8. Becker, J., Wieser, C., Fell, S. & Steiner, K. (2011). A multi-scale approach to material modeling of fuel cell diffusion media. *Int. J. Heat Mass Transfer* **54**(7–8), 1360-1368.
9. Wiegmann, A. & Zemitis, A. (2006). EJ-HEAT: A Fast Explicit Jump Harmonic Averaging Solver for the Effective Heat Conductivity of Composite Materials. Report Nr. 94, Fraunhofer Institute ITWM, Kaiserslautern, Germany, 2006.
10. Warner, S.B. (1995). *Fiber Science*. Prentice-Hall, Englewood Cliffs.
11. Morton, W.E. & Hearle, J.W.S. (2008). *Physical properties of textile fibres*, Fourth ed. Woodhead Publishing Limited, Cambridge, England.
12. Pradere, C., Batsale, J.C., Goyhénèche, J.M., Pailler, R. & Dilhaire, S. (2009). Thermal properties of carbon fibers at very high temperature. *Carbon* **47**(3), 737-743.
13. (2005). *Springer Handbook of Condensed Matter and Materials Data*, W. Martienssen, H. Warlimont (Eds.). Springer, Berlin, Germany.
14. Mansour, N.N., Panerai, F., Martin, A., Parkinson, D.Y., MacDowell, A.A., Fast, A., Vignoles, G. & Lachaud, J. (2013). A new approach to light-weight ablators analysis: from micro-tomography measurements to statistical analysis and modeling. In Proc. *44th AIAA Thermophysics Conference*, American Institute of Aeronautics and Astronautics, AIAA 2013-2768. doi:10.2514/6.2013-2768.
15. Lachaud, J. & Vignoles, G.L. (2009). A Brownian motion technique to simulate gasification and its application to C/C composite ablation. *Computational Materials Science* **44**(4), 1034-1041.
16. Lachaud, J. & Mansour, N.N. (2010). Microscopic Scale Simulation of the Ablation of Fibrous Materials. In Proc. *48th AIAA Aerospace Sciences Meeting Including the New Horizons Forum and Aerospace Exposition*, American Institute of Aeronautics and Astronautics, AIAA Paper N. 2010-984. doi:10.2514/6.2010-984.